

Use of Numerical Simulation for Growing High Quality Sapphire Crystals by the Kyropoulos method

S.E. Demina*¹, E.N. Bystrova¹, V.S. Postolov², E.V. Eskov², M.V. Nikolenko², D.A. Marshanin², V.S. Yuferev³, V.V. Kalaev⁴

¹ *Soft-Impact, Ltd, P.O. Box 83, 194156, St. Petersburg, Russia*

² *Monocrystal Inc., 355035, Stavropol, Russia*

³ *Ioffe Physico-Technical Institute, 194021 St. Petersburg, Russia*

⁴ *Semiconductor Technology Research GmbH, Eltersdorferstr. 22, 91058 Erlangen, Germany*

Abstract

In the present work, an advanced numerical model is suggested to analyze heat transfer and flow pattern in sapphire crystal growth by the Kyropoulos technique. The new approach accounts for radiative heat exchange in the crystal, convection in the melt and provides prediction of the crystallization front shape. The model allowed the analysis of several growth setup designs and selection of an optimal configuration. The numerical predictions performed with the CGSim software (www.semitech.us) agree well with available experimental data obtained in optimized crystal growth process reported for the first time.

PACS: 47.27Te; 47.27Eq; 81.10Aj; 81.10Fq

Keywords: A1. Computer Simulation; A1. Mass transport; A2. Kyropoulos method; B1. Sapphire

1. Introduction

Recent progress in high-power light-emitting diode production requires growing high quality sapphire crystals of larger size and weight and increasing the efficiency of sapphire growth technologies. A modified Kyropoulos method developed by *Monocrystal, Inc.* is a promising technique to solve such issues via adjustments of the hot zone to get optimization of the crystallization front shape and the crystallization rate. Such adjustments were provided experimentally with an efficient support of numerical simulation [1-4] helped to evaluate different hot zone modification.

In the literature, there is a good experience of modeling of oxide crystal growth by Czochralski and Bridgman techniques [5-10]. However, the growth of sapphire by the Kyropoulos method is poorly studied today and considered, to our knowledge, within a conjugated approach in the present paper and in Ref. [11] only. In the paper [11], we reported first experience in the simulations as well as a verification of crystallization front prediction for a shouldering stage. In the present work: (i) the mathematical model is described in detail; (ii) another crystal height is considered; (iii) new ideas described in both papers are tested experimentally and the results are presented for the first time.

The computations have been made using the CGSim program package [12]. Kyropoulos crystal growth is numerically considered with a 2D axisymmetric approach accounting for the heat transfer in the whole system as well as radiative heat exchange in the semitransparent crystal, melt convection, and crystallization front formation in the crystallization zone. The simulation studies the effect of growth parameters and design of the reactor elements on the temperature field, the crystallization front shape, temperature gradient distribution, and thermal stresses in the crystal. Special attention is given to an analysis of the melt flow, which can help to reduce temperature gradients in the crystal and control the transport of bubbles. The results of numerical simulation and respective experimental crystal growth for optimized heat transfer parameters will be presented in our paper.

*Corresponding author. Tel.: +7(812) 320-4390; fax: +7(812) 326-6194.
E-mail address: Svetlana.Demina@str-soft.com

2. Model

The approach we suggest requires a pre-computation of the global heat transfer in the whole system, considering all furnace elements. After that, heat exchange is modeled only in the crystallization zone, including the crystal, melt, crucible, and a gas region around the crystal. The computation in the limited zone involves the turbulent flow of the sapphire melt, the laminar gas flow, and radiative heat exchange in the semitransparent crystal.

2.1. Model of global heat exchange in the whole system

To compute global heat transfer, we used the axisymmetric model suggested in Ref. [1]. The crystal is assumed to be opaque and the melt to be solid with the effective thermal conductivities. The model accounts for the heat transfer via conduction and heat exchange between solid elements by radiation. To account for the heat transfer within solid domains a finite-volume numerical algorithm has been used. According to this algorithm, the balance equation is written as

$$\nabla \cdot (\lambda \nabla T) - q = 0, \quad (1)$$

where q is a volume source of the heat generation, λ is the thermal conductivity depending on the temperature T . Radiative heat exchange between any solid surfaces through a non-participating medium is computed in terms of gray-diffusive surface radiation. The heat-balance equation on the boundary between solid and transparent domains can be written in accordance with the Stephan-Boltzman law as

$$q_k^{out} = \varepsilon_k \sigma T_k^4 + (1 - \varepsilon_k) q_k^{in}, \quad (2)$$

where q_k^{out} and q_k^{in} is the outgoing and incoming radiation flux, respectively, ε_k is the emissivity, $\sigma = 5.67 \cdot 10^{-8} \text{ W}/(\text{m}^2 \cdot \text{K}^4)$ is the Stephan-Boltzman constant, and k is the cell index (the elementary surface element). The total radiative flux incoming on a given surface element is calculated using the configuration factors F_{ij} . In framework of this method, the incoming radiation flux can be calculated as

$$q_k^{in} = \sum_{j=1}^N q_j^{out} F_{kj}, \quad (3)$$

where F_{kj} is the configuration factor depending on the reactor design and the generated computational grid.

The fixed temperature value $T = \text{const}$, known from thermal measurements in the cooling system, was set as boundary conditions along external boundaries of the computational domain.

2.2. Model of heat transfer and mass transport in the crystallization zone

The heat transfer and melt convection in the crystallization zone were computed using the approach described in Refs. [2, 3]. In the frame of this approach, heat transfer is considered via conduction and radiation. The governing differential equations of heat transfer with radiative heat exchange in the crystal and mass transport are as follows:

$$\nabla \cdot \vec{u} = 0 \quad (4)$$

$$\rho \frac{d\vec{u}}{dt} = -\nabla p + \nabla \cdot (2\mu_{eff} \dot{S}) + \rho \beta (T_0 - T) \vec{g} \quad (5)$$

$$\rho C_p \frac{dT}{dt} = \nabla \cdot (\lambda_{eff} \nabla T) - \nabla \cdot \vec{q}_r \quad (6)$$

Here, ρ is the density, \vec{u} is the velocity, \vec{g} is the gravity vector, p is the pressure, \vec{q}_r is the vector of net radiative heat flux, β is the thermal expansion coefficient, \dot{S} is the strain-rate tensor, $\mu_{eff} = \mu_{molecular} + \mu_t$ is the effective dynamic viscosity, C_p is the specific heat, T is the temperature, $T_0 =$

2227 K is the sapphire melting temperature, $\lambda_{eff} = \lambda + \frac{\mu_t}{Pr_t}$ is the effective thermal conductivity, and $Pr_t=0.9$ is the turbulent Prandtl number. The source term in Eq. (6) on the right is the divergence of the net radiative heat flux, which can be found from the following expression:

$$\vec{q}_r(\vec{r}) = \int_{4\pi} I(\vec{r}, \vec{\Omega}) \vec{\Omega} d\vec{\Omega}, \quad (7)$$

where $I = I(\vec{r}, \vec{\Omega})$ is the radiative intensity at the point $\vec{r} = (x, y, z)$ in the direction $\vec{\Omega} = (\Omega_x, \Omega_y, \Omega_z)$ see for details Fig. 4 in Ref. [13]. The value I is found by solving the radiative transfer equation in semitransparent sapphire crystal as described below in *Item 2.3* in detail. In accordance with an algebraic turbulence model, the turbulent viscosity in the melt has been found as

$$\mu_t = C_1 \rho y^2 \sqrt{2SS + \frac{1}{Pr_t} \frac{1}{\rho} |\vec{g} \cdot grad\rho|}, \quad (8)$$

where y is the distance to the closest solid wall, $SS = S_{ij}S_{ij}$, $S_{ij} = \frac{1}{2} \left(\frac{\partial u_i}{\partial x_j} + \frac{\partial u_j}{\partial x_i} \right)$ is the square strain rate tensor, and $C_1 = 0.063$ is an empirical constant. The component $\frac{1}{Pr_t} \frac{1}{\rho} |\vec{g} \cdot grad\rho|$ accounts for turbulence generation via buoyancy.

Crystallization rate calculation

The crystallization rate can be calculated as follows:

$$V_{crys} = \frac{1}{\rho_{crys} \Delta H} \left(\lambda_{crys} \frac{\partial T_{crys}}{\partial n} - \tilde{q}_{rad} - \lambda_{melt} \frac{\partial T_{melt}}{\partial n} \right), \quad (9)$$

where ρ_{crys} is the crystal density, ΔH is the latent heat, $\lambda_{crys/melt}$ are the thermal conductivities in the crystal/melt, \tilde{q}_{rad} is the density of net radiative flux in the range of sapphire semitransparency, and n is the normal to the crystallization front.

2.3. Model of radiative heat transfer in semitransparent sapphire crystal

The steady-state equation of radiative transport in the Cartesian coordinates x, y, z without scattering is

$$\Omega \cdot \nabla I + k I \equiv \Omega_x \frac{\partial I}{\partial x} + \Omega_y \frac{\partial I}{\partial y} + \Omega_z \frac{\partial I}{\partial z} + k I = F, \quad (10)$$

where $I = I(\vec{r}, \vec{\Omega})$ is the radiative intensity at the point $\vec{r} = (x, y, z)$ in the direction $\vec{\Omega} = (\Omega_x, \Omega_y, \Omega_z)$, k is the absorption coefficient, $F = kI_b$, $I_b = n^2 \sigma T^4 / \pi$ is the black body radiation intensity, T is the temperature, and n is the refraction coefficient. The scattering is supposed to be zero here. Boundary conditions for radiative transport are described in details in Refs. [3-6].

3. Results

The suggested approach has been initially tested on a simplified reactor design, the so-called model furnace, as well as on several modifications of the real industrial growth setup.

The simplified model furnace is presented as an illustration of global heat transfer modeling with a detailed analysis of the heat flux distribution. Fig. 1 shows the heat flux vector (a) and the temperature distribution (b) in the model furnace. We have successfully verified the computations of global heat transfer by comparing the integrated heat fluxes calculated along water-cooled chamber walls, using the

measured temperature difference between inlet and outlet water for three separate segments of the chamber.

For an industrial growth setup, we have made series of computations, varying parameters and design of the furnace elements. Global heat transfer, heat transfer in the hot zone with radiative heat exchange in the crystal and melt convection together with the crystallization front formation, thermal stresses in the crystal were analyzed for all modifications. Special attention was given to the analysis of the melt flow patterns. The height of the cylindrical part of the considered crystal was 34 mm, the melt depth from the free surface was 169 mm. The following optical properties were used in our computations: the transparent band was 0.5-4.5 μm with an absorption coefficient of 19.26 m^{-1} ; the refractive index was 1.78. The physical properties of solid and fluid sapphire used in the computations in the local crystallization zone (Fig. 2) are given in Table 1.

It was found that a dominating flow structure is two-vertex for most modifications during the growth of the upper crystal part as shown in Case 1 ((Fig. 2(a)). One can observe a large vortex occupying practically the whole melt core and a secondary vortex of lower intensity, which arises near the melt free surface during beginning of the crystal growth and disappears at a certain cylindrical growth stage. Note that the vortices are counter rotating. The larger vortex has a direction which can provide the formation of crystallization front with a conical shape, while the secondary vortex can change the crystal shape and lead to a so-called remelting zone ((Fig. 3(a)). A target of our parametric study was to eliminate the two-vortex structure to decrease the temporal remelting area along the melt-crystal interface. The overheating of the side crystal surface reported in Ref. [7] was not observed in all our calculations.

After testing many changes in growth technology, a way to improve the flow has been found. Modifications of the heat shield system with the utilization of alternative materials could provide changes of the temperature in the hot zone. As a result, the melt temperature gradient decreases and the melt flow becomes less intensive and more uniform (see Case 2, Fig. 2(b)). Moreover, the temperature gradient in the crystal also decreases. This is clearly seen in Fig. 4, which shows the 1D temperature gradient distribution along the crystallization front for both modifications. Note that the crystallization front has a higher deflection and the cylindrical growth is stabilized sooner than in Case 1. The thermal stress distribution in the crystal for both cases is illustrated in Fig. 5. Maximal values of the stresses are in the same locations as in the gradient distribution, in particular, along the crystallization front, near the seed, and bottleneck. It is shown that the thermal stresses along the crystallization front are lower in Case 2 by about 30 % in comparison with Case 1.

Based on the computational data, the industrial furnace has been optimized and a crystal having a lower area of the remelting zone and higher quality has been grown (Fig. 3(b)) in the modified setup, which indicates the high prediction accuracy of the developed computer model.

4. Conclusion

We have presented a numerical approach for the simulation of single sapphire crystal growth by the Kyropoulos method. This approach uses a minimal set of simplifications and estimates the temperature at any point of the furnace, which is very difficult to do experimentally. In addition, the model accounts for the effects of the parameters and design of the reactor parts on the temperature fields. Moreover, the model can estimate the temperature gradient in the crystal and in the melt, the heat flux distribution depending on the materials of the furnace parts, geometry of the crystallization front, and the power consumption. The model has been tested using the industrial furnace developed by *Monocrystal, Inc.* The good agreement between the computations and the data indicates an adequate prediction of the temperature fields in the reactor. With these findings of the global heat transfer and crystallization front formation, *Monocrystal, Inc.* has designed an experimental growth reactor with the modifications of the reactor parts to produce sapphire crystals of better quality. New engineering ideas are now actively tested using numerical simulation before their experimental realization for the growth of sapphire crystals of a larger height and diameter.

5. References

- [1] E. Yakovlev, V. Kalaev, I. Evstratov, Ch. Frank, M. Neubert, P. Rudolph, Yu. Makarov, J. Crystal Growth, 252/1-3 (2003) pp. 26-36.
- [2] D. Lukanin, V. Kalaev, Yu. Makarov, T. Wetzel, J. Virbulis, and W. von Ammon, J. Crystal Growth, 266/1-3 (2004) pp. 20 – 27.
- [3] V. Mamedov, S. Rukolaine, Proc. of Int. Symp. on Radiation, 2004, 21-25 June, Istanbul, Turkey, pp. 69-78.
- [4] V. Yuferev, O. Budenkova, M. Vasiliev, S. Rukolaine, V. Shlegel, Ya. Vasiliev, A. Zhmakin, J. Crystal Growth 253 (2002) 383.
- [5] O. Budenkova, M. Vasiliev, V. Yuferev, E. Bystrova, V. Kalaev, V. Bermúdez, E. Diéguez and Yu. N. Makarov, J. Crystal Growth 266 (2004) 103
- [6] O. Budenkova, M. Vasiliev, V. Mamedov, V. Yuferev, V. Kalaev, J. Crystal Growth 303 (2007) 156
- [7] Qiang Xiao, Jeffrey J. Derby, J. Crystal Growth 139 (1994) 147.
- [8] A. Hayashi, V. Kobayashi, C. Jing, T. Tsukado, M. Hozawa, Int. J. Heat and Mass Transfer, 47 (2004) 5501.
- [9] D. Schwabe, R. R. Sumathi, H. Wilke, J. Crystal Growth 265 (2004) 494.
- [10] S. Brandon, J. J. Derby. J. Crystal Growth, 121 (1992) 473-494.
- [11] S. Demina, E. Bystrova, M. Lukanina, V. Mamedov, V. Yuferev, E. Eskov, M. Nikolenko, V. Postolov, V. Kalaev, Optical Materials 30 (2007) 62–65.
- [12] http://www.semitech.us/products/cz_growth_simulator/
- [13] V. Yuferev, O. Budenkova, M. Vasiliev, S. Rukolaine, V. Shlegel, Ya. Vasiliev, A. Zhmakin, J. Crystal Growth 253 (2003) 387 – 397.
- [14] H. Kopetsch, J. Crystal Growth 102 (1990), 505–528.
- [15] W. E. Langlois, J. Crystal Growth 48 (1980), 25–28.
- [16] Internal reports of *Monocrystal Inc.*, Stavropol (Russia), www.monocrystal.com

6. Tables

Table 1. Sapphire properties used in analyzing the crystallization zone, mainly taken from Refs. [14 – 16].

Property	Value
<i>Thermal conductivity of the crystal, W/(m·K)</i>	5
<i>Thermal conductivity of the melt, W/(m·K)</i>	2.05
<i>Specific heat of the crystal, J/(kg·K)</i>	1430
<i>Specific heat of the melt, J/(kg·K)</i>	1260
<i>Density of the crystal, kg/m³</i>	3970
<i>Density of the melt, kg/m³</i>	3030
<i>Emissivity of the crystal</i>	0.869
<i>Emissivity of the melt</i>	0.33
<i>Melting temperature, K</i>	2327
<i>Solidification heat, J/kg</i>	1407000
<i>Dynamic viscosity, kg/(m·c)</i>	0.057
<i>Thermal expansion, 1/K</i>	5.0e-6
<i>C11, Pa</i>	49.6e10
<i>C12, Pa</i>	14.8e10

7. Figures

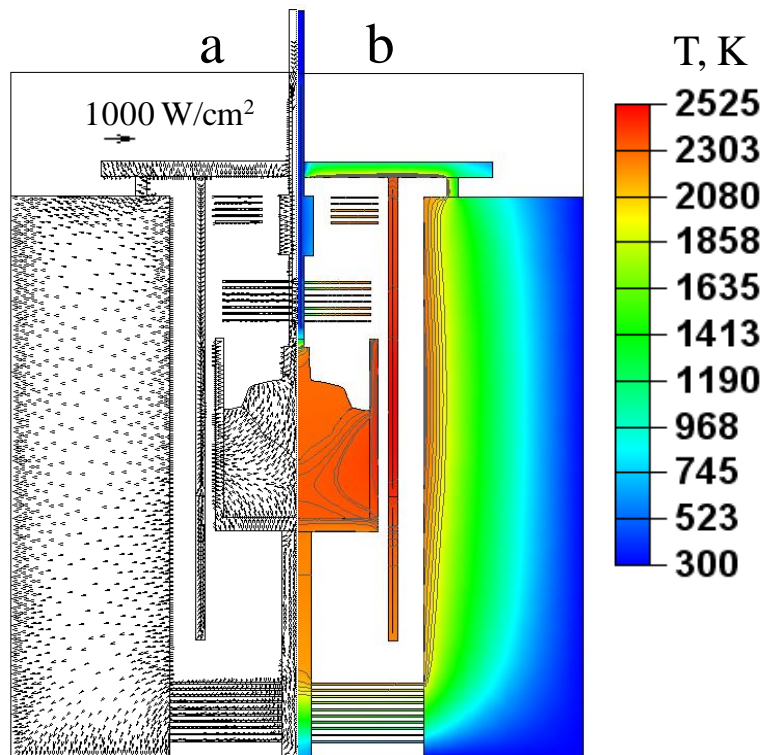


Fig. 1. The distribution of the heat flux vectors (a) and the temperature (b) in the model furnace.

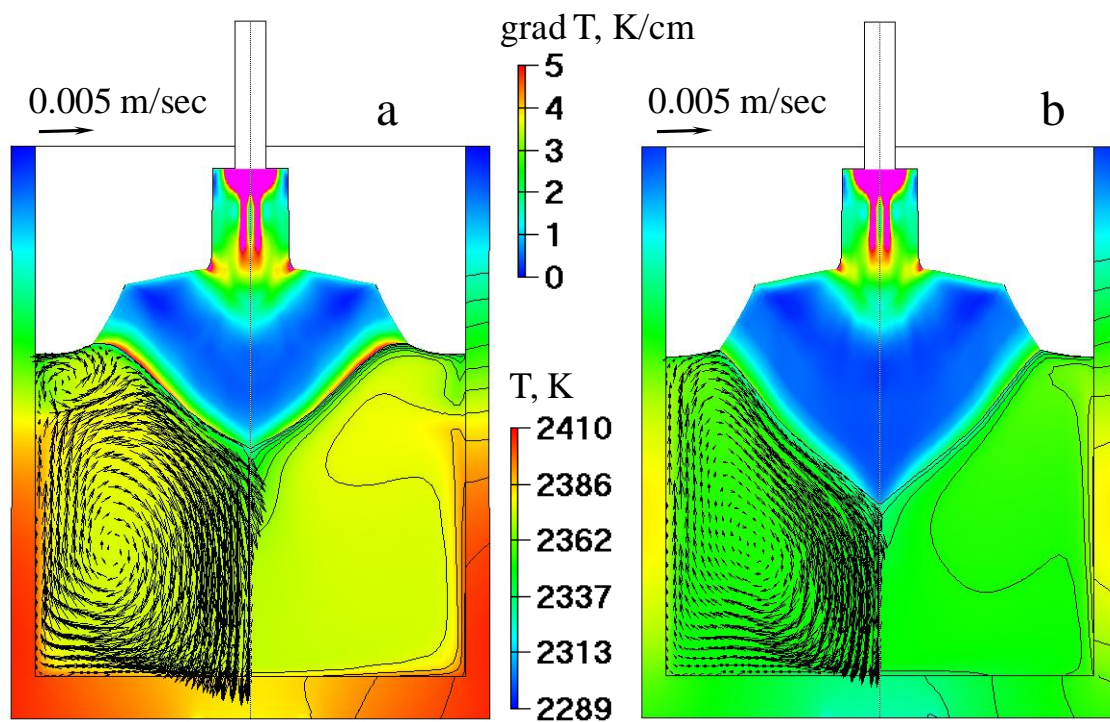


Fig. 2. The temperature gradient distribution in the crystal, the temperature distribution in the crystallization zone, and the flow pattern in the melt by vectors in the industrial furnace for Case 1 (a) and Case 2 (b).

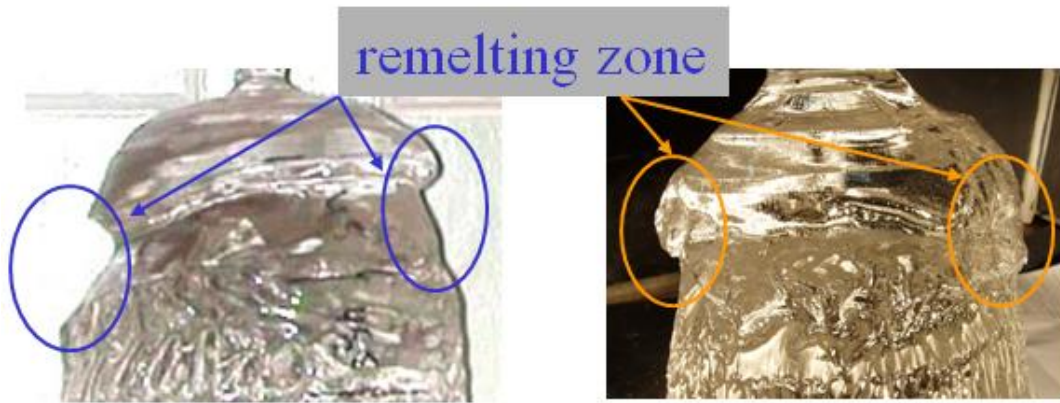


Fig. 3. The top part of sapphire boules with a larger (left) and a smaller (right) remelting zones.

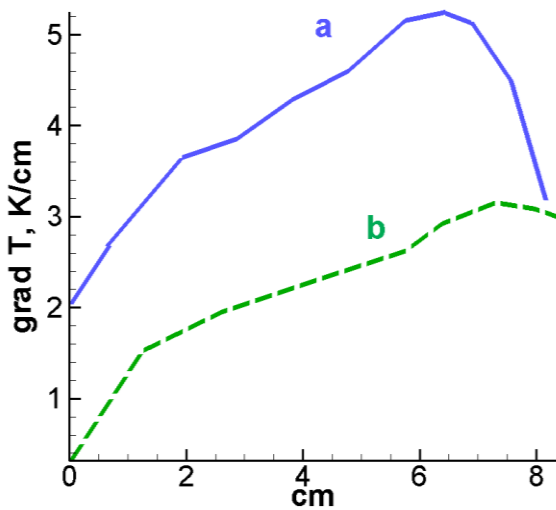


Fig. 4. The 1D temperature gradient distribution along the crystallization front for Case 1 (a) and Case 2 (b).

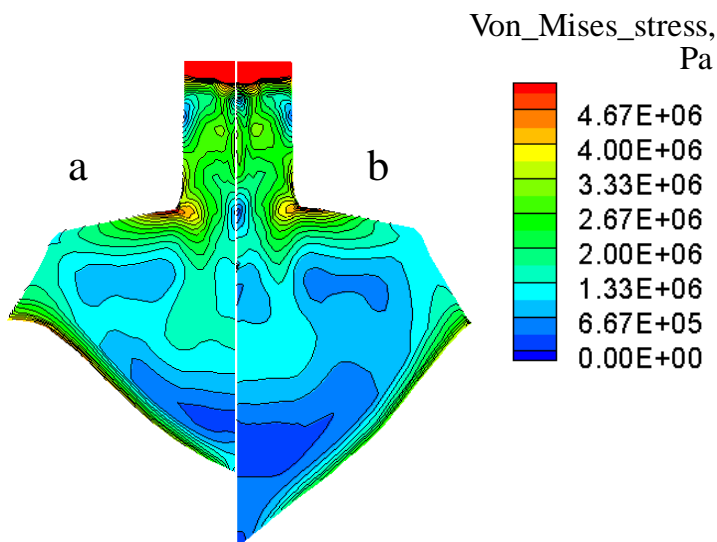


Fig. 5. The distribution of Von Mises thermal stress norm in the crystal for Case 1 (a) and Case 2 (b).